Current Biology, Volume *31*

Supplemental Information

Ligation of newly replicated DNA controls the timing of DNA mismatch repair

Gloria X. Reyes, Anna Kolodziejczak, Lovely Jael Paul Solomon Devakumar, Takashi Kubota, Richard D. Kolodner, Christopher D. Putnam, and Hans Hombauer

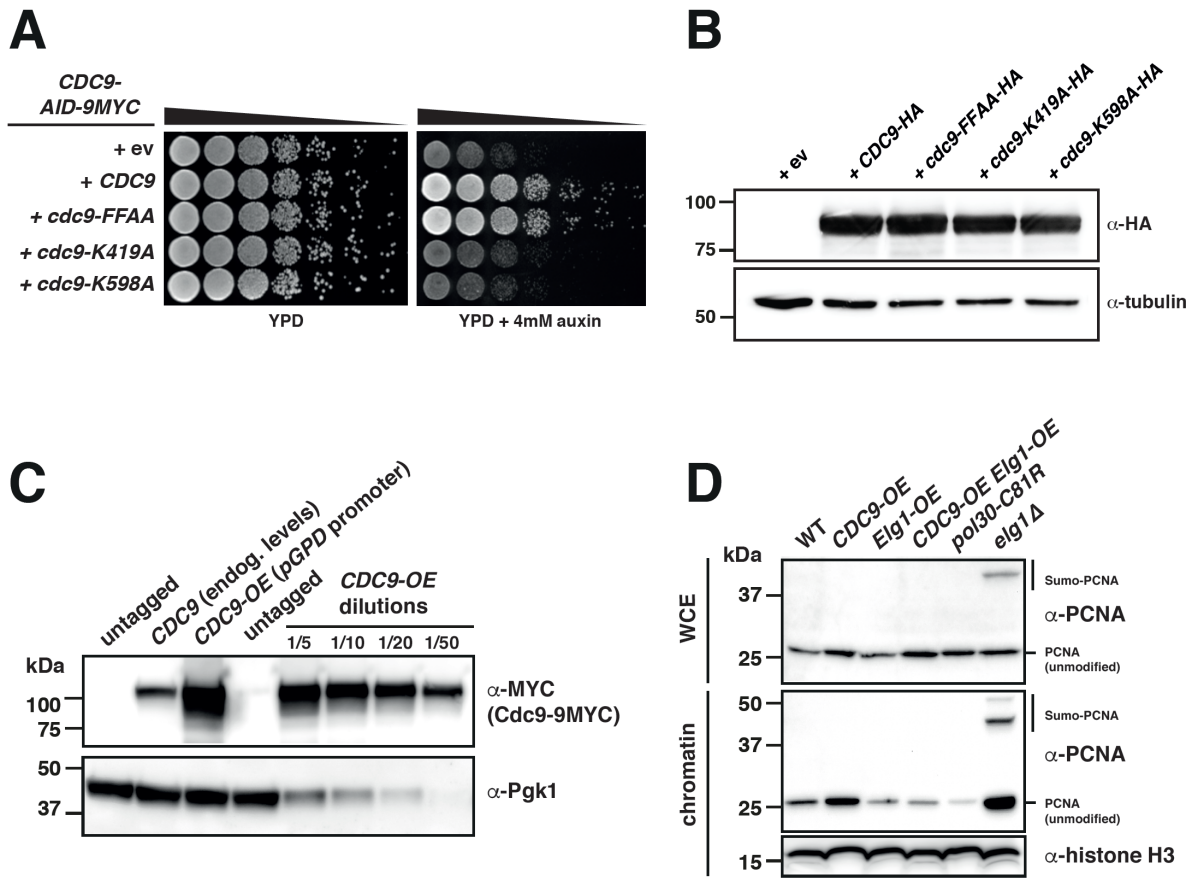

Figure S1. Validation of the function of plasmid-borne *CDC9* alleles and characterization of *CDC9* overexpressing strains. Related to Figure 1, 2 and 3 and Table S2.

(A) High copy number vectors were tested for their ability to complement a chromosomally encoded version of *CDC9* fused to the auxin-inducible degron. Plasmids expressing WT *CDC9* or *cdc9-FFAA*, which encodes a version of Cdc9 that cannot interact with PCNA *in vitro,* allowed cells to grow on YPD containing 4 mM auxin. In contrast, an empty vector (ev) control and both ligase-defective mutant alleles (*cdc9-K419A* and *cdc9-K598A*) could not. (B) Western blot analysis indicating expression levels of WT-Cdc9 or *cdc9* mutant alleles (tagged with a C-terminal HA-tag) expressed from high copy number plasmids. An antibody against tubulin was used as a loading control. (C) Western blot analysis showing Cdc9 protein levels in yeast strains expressing the *CDC9* gene at endogenous levels (endog. levels) or under the control of the strong constitutive promoter (pGPD), resulting in Cdc9-overexpression (*CDC9-OE*). To facilitate the visualization of the Cdc9 protein, the chromosomal *CDC9* gene was tagged at the C-terminus with a 9xMYC tag. (D) Abundance of PCNA in whole cell extracts (WCE) and chromatin-enriched fractions (chromatin) in the indicated mutant strains. Strains carrying the *pol30-C81R* and *elg1Δ* mutations, which were previously shown to have reduced or increased chromatin-bound PCNA levels, respectively [S1, S2], were included as controls. Inactivation of Elg1 results in an increase of Sumo-PCNA as previously reported [S2, S3]. Histone H3 was used as a chromatin-loading control.

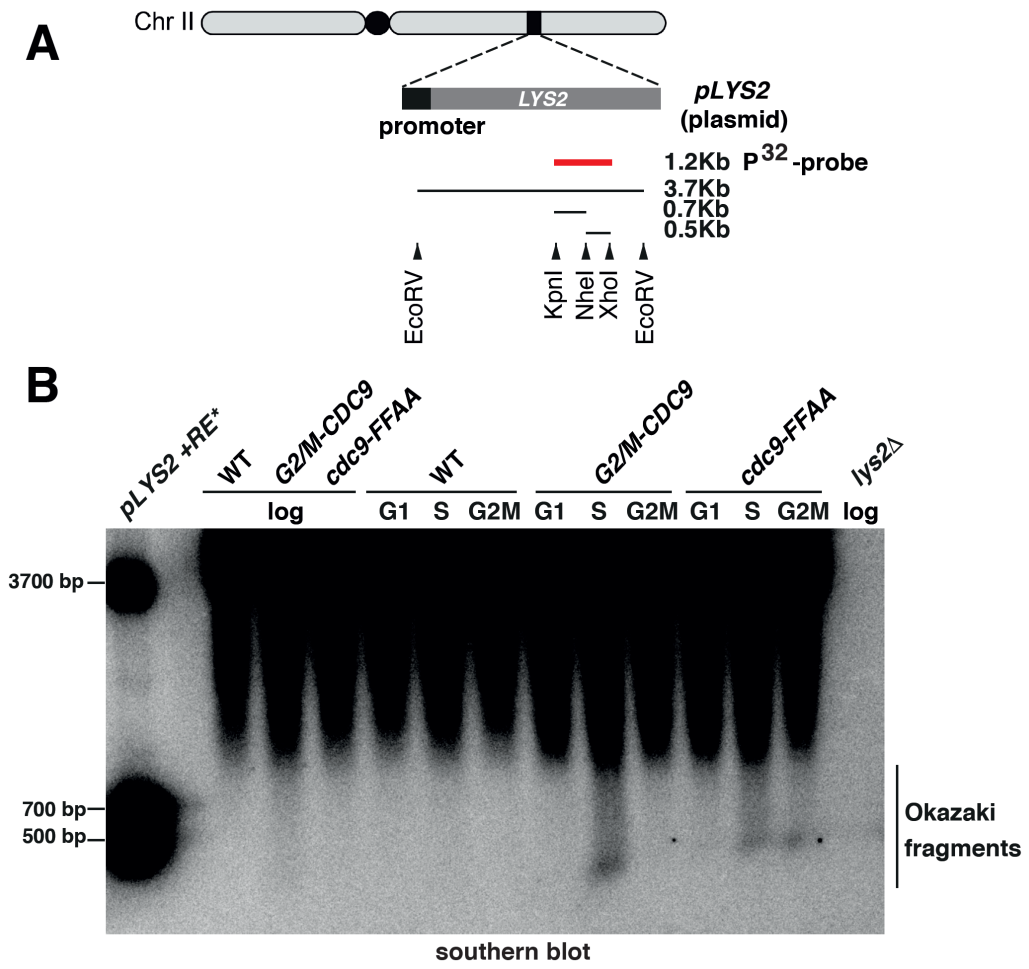

Figure S2. *CDC9* alleles with delayed (*G2/M-CDC9*) or reduced (*cdc9-FFAA*) ligase activity results in accumulation of unprocessed Okazaki fragments at the *LYS2* locus. Related to Figure 4.

(A) Diagram showing the strategy used for the generation of the P^{32}-probe used for detection of Okazaki fragments at the *LYS2* locus by Southern blotting. (B) Southern blot analysis used for the detection of Okazaki fragments at the *LYS2* locus in WT and the *G2/M-CDC9* or the *cdc9-FFAA* mutant strains either growing logarithmically (log), arrested in G1 phase by alpha-factor (α-F), synchronized in S phase (30 min release after α-F) or synchronized in G2/M phase (90 min release after α-F). A *LYS2* deficient strain (*lys2Δ*) was used as a control for *LYS2*-P^{32} probe specificity. As a positive control, a plasmid harboring the *LYS2* gene was digested with either *EcoR* V (detected as a 3.7 kb fragment) or *Kpn* I +*Nhe* I +*Xho* I (detected as 0.5 and 0.7 kb fragments) and pooled (*pLYS2+RE**).

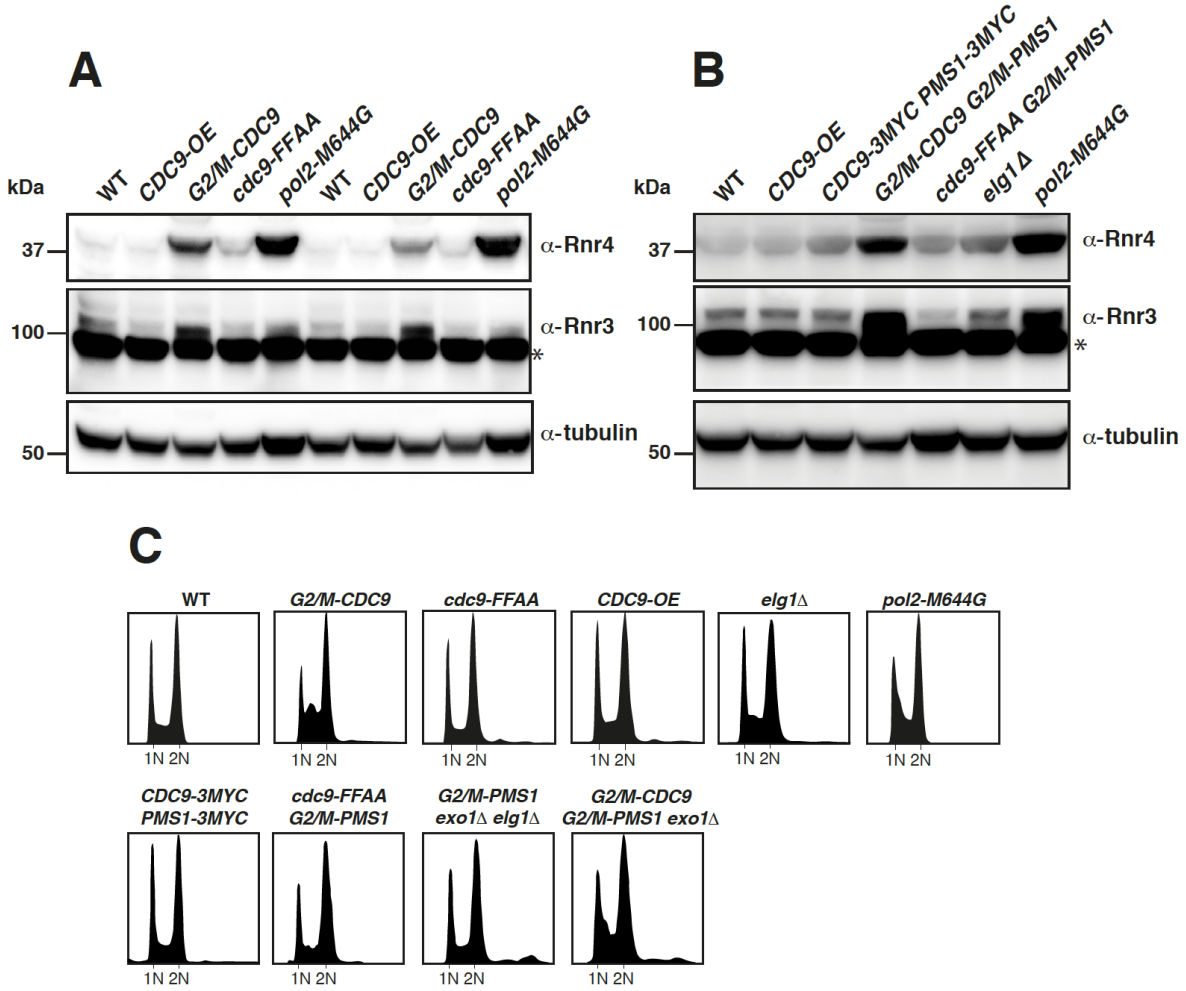

Figure S3. Delayed ligation of Okazaki fragments in the *G2/M-CDC9* mutant results in activation of the DNA damage response and accumulation of cells in S phase.
Related to Figure 4.
(A, B) Whole cell lysates of the indicated strains were analyzed by western blotting with antibodies recognizing DNA damage-inducible ribonucleotide reductase subunits Rnr3 and Rnr4 [S4, S5]. A mutant strain expressing the *pol2-M644G* allele that results in activation of the DNA damage response [S6, S7] was included as a positive control. * denotes a cross-reacting protein. Tubulin was used as a loading control. (C) DNA content analysis of the indicated logarithmically growing strains.

	Mutation Rate (fold increase)*		
Relevant genotype	**Ura$^+$ Lys$^+$**	**Ura$^+$ Thr$^+$**	**Ura$^+$ Can^R**
wild-type + pRS426	1.1 [0.8-2.8] x 10^{-7} (1)	1.5 [0.8-2.6] x 10^{-8} (1)	7.7 [4.4-16.8] x 10^{-7} (1)
wild-type + pRS426-*CDC9*	1.0 [0.5-1.8] x 10^{-6} (9)	6.8 [3.3-11.4] x 10^{-8} (4)	2.0 [1.5-2.5] x 10^{-6} (3)
exo1Δ + pRS426	3.0 [1.3-6.1] x 10^{-7} (3)	1.6 [0.6-2.2] x 10^{-8} (1)	2.5 [2.2-3.2] x 10^{-6} (3)
exo1Δ + pRS426-*CDC9*	1.0 [0.7-1.6] x 10^{-4} (940)	2.2 [1.8-3.1] x 10^{-6} (144)	9.4 [6.2-21.7] x 10^{-6} (12)
exo1Δ + pRS426-*cdc9-F44A-F45A*	4.1 [2.2-8.1] x 10^{-6} (38)	6.4 [4.7-11.9] x 10^{-8} (4)	3.6 [2.8-4.4] x 10^{-6} (5)
exo1Δ + pRS426-*cdc9-K419A*	2.7 [1.3-4.6] x 10^{-7} (2)	1.6 [1.3-2.6] x 10^{-8} (1)	2.5 [1.8-3.7] x 10^{-6} (3)
exo1Δ + pRS426-*cdc9-K598A*	4.1 [2.6-9.5] x 10^{-7} (4)	1.8 [0.8-3.2] x 10^{-8} (1)	2.6 [1.9-3.4] x 10^{-6} (3)

Table S1. Mutation rate analysis in strains overexpressing WT-*CDC9* and *cdc9* mutant alleles. Related to Figure 1A.

* Median rates of *lys2-10A* (Ura$^+$ Lys$^+$) and *hom3-10* (Ura$^+$ Thr$^+$) frameshift reversion and inactivation of *CAN1* gene (Ura$^+$ Can^R) assays with 95% confidence interval in square brackets and fold increase relative to the wild-type in parentheses.

	Mutation Rate (fold increase)*		
Relevant genotype	**Lys$^+$**	**Thr$^+$**	**Can^R**
wild-type	1.5 [0.8-2.2] x 10^{-8} (1)	2.1 [1.4-3.2] x 10^{-9} (1)	7.2 [5.7-9.0] x 10^{-8} (1)
msh2Δ	9.9 [8.1-10.8] x 10^{-5} (6771)	6.3 [5.2-12.8] x 10^{-6} (3053)	5.4 [4.4-7.2] x 10^{-6} (75)
CDC9-OE	6.0 [4.6-6.9] x 10^{-8} (4)	5.4 [4.2-6.3] x 10^{-9} (3)	1.1 [0.8-1.4] x 10^{-7} (2)
exo1Δ	9.8 [6.9-22.8] x 10^{-8} (7)	5.2 [3.3-7.9] x 10^{-9} (3)	4.3 [2.9-8.7] x 10^{-7} (6)
CDC9-OE exo1Δ	6.1 [3.4-12.1] x 10^{-6} (416)	3.7 [2.8-5.7] x 10^{-7} (180)	1.3 [1.1-1.5] x 10^{-6} (18)
exo1-FFAA-Δ571-702	3.6 [2.9-5.3] x 10^{-8} (2)	2.8 [2.0-4.7] x 10^{-9} (1)	8.2 [6.3-17.5] x 10^{-8} (1)
CDC9-OE exo1-FFAA-Δ571-702	6.7 [4.4-10.8] x 10^{-6} (457)	3.4 [1.6-5.6] x 10^{-7} (163)	1.7 [0.7-2.8] x 10^{-6} (24)
pol30-K217E	1.2 [0.8-2.4] x 10^{-6} (85)	4.1 [3.5-6.4] x 10^{-8} (20)	5.1 [3.9-10.7] x 10^{-7} (7)
pol30-K217E exo1Δ	5.5 [4.8-7.0] x 10^{-5} (3772)	2.7 [1.6-4.2] x 10^{-6} (1317)	7.1 [3.7-10.8] x 10^{-6} (99)
CDC9-OE pol30-K217E	6.9 [6.1-9.5] x 10^{-6} (474)	2.1 [1.5-3.1] x 10^{-7} (103)	1.2 [1.0-1.3] x 10^{-6} (16)
CDC9-OE exo1Δ pol30-K217E	3.0 [2.2-4.2] x 10^{-4} (20751)	2.1 [1.4-3.3] x 10^{-5} (10089)	2.0 [1.4-3.1] x 10^{-5} (278)
pms1-A99V	4.0 [1.7-7.3] x 10^{-7} (27)	6.3 [4.0-9.7] x 10^{-8} (30)	4.0 [1.9-7.5] x 10^{-7} (6)
CDC9-OE pms1-A99V	7.9 [3.4-12.4] x 10^{-6} (543)	1.4 [0.7-2.2] x 10^{-6} (688)	1.5 [1.1-1.7] x 10^{-6} (20)
CDC9-OE msh2Δ	1.2 [0.6-2.0] x 10^{-4} (7948)	1.4 [0.9-2.1] x 10^{-5} (6533)	2.9 [1.1-3.7] x 10^{-5} (405)
rnh201Δ	2.1 [1.7-3.3] x 10^{-8} (2)	5.5 [4.2-7.4] x 10^{-9} (3)	1.3 [0.8-1.9] x 10^{-7} (2)
CDC9-OE rnh201Δ	9.6 [7.2-20.0] x 10^{-8} (7)	2.6 [1.9-3.2] x 10^{-8} (13)	6.0 [3.1-10.0] x 10^{-7} (8)
exo1Δ rnh201Δ	2.0 [1.3-3.3] x 10^{-7} (14)	1.7 [1.2-3.1] x 10^{-8} (8)	8.0 [6.7-10.0] x 10^{-7} (11)
CDC9-OE exo1Δ rnh201Δ	1.0 [0.5-2.0] x 10^{-5} (716)	1.2 [0.7-1.8] x 10^{-6} (561)	4.7 [1.8-6.6] x 10^{-6} (66)
ELG1-OE	5.8 [4.2-8.2] x 10^{-7} (40)	8.5 [5.4-16.5] x 10^{-9} (4)	4.4 [3.4-6.0] x 10^{-7} (6)
ELG1-OE exo1Δ	6.5 [4.9-8.5] x 10^{-7} (45)	4.7 [3.2-9.5] x 10^{-8} (23)	1.5 [1.0-2.0] x 10^{-6} (21)
CDC9-OE ELG1-OE	5.6 [2.8-11.9] x 10^{-7} (38)	2.3 [1.4-3.2] x 10^{-8} (11)	5.6 [3.1-9.8] x 10^{-7} (8)
CDC9-OE exo1Δ ELG1-OE	5.0 [2.8-7.3] x 10^{-5} (3387)	5.8 [3.5-9.1] x 10^{-6} (2809)	2.1 [1.5-3.6] x 10^{-5} (294)
elg1Δ	1.0 [0.7-1.9] x 10^{-7} (7)	4.8 [3.4-10.2] x 10^{-9} (2)	1.8 [1.5-2.3] x 10^{-7} (3)
CDC9-OE elg1Δ	2.3 [1.5-3.2] x 10^{-7} (16)	8.6 [5.8-11.1] x 10^{-9} (4)	3.4 [1.7-8.6] x 10^{-7} (6)
exo1Δ elg1Δ	1.5 [0.7-2.2] x 10^{-7} (10)	1.7 [1.4-2.6] x 10^{-8} (8)	7.8 [6.0-12.3] x 10^{-7} (11)
CDC9-OE exo1Δ elg1Δ	7.0 [4.2-11.7] x 10^{-7} (48)	7.4 [4.5-11.1] x 10^{-7} (355)	3.2 [1.9-4.4] x 10^{-6} (44)

Table S2. Increased Cdc9 ligase activity interferes with Exo1-dependent and Exo1-independent MMR. Related to Figure 2 and 3.

* Median rates *lys2-10A* (Lys$^+$) and *hom3-10* (Thr$^+$) frameshift reversion assays and inactivation of the *CAN1* gene (Can^R) with 95% confidence interval in square brackets and fold increase relative to the wild-type in parentheses.

	WT*	*CDC9-OE*	*exo1-F447A-F448A -Δ571-702*	*CDC9-OE exo1-F447A-F448A -Δ571-702*	*CDC9-OE msh2Δ*	*msh2Δ***
Can^R clones sequenced	92	119	101	92	97	164
Mutations overall	92 (100.0)	119 (100.0)	101 (100.0)	92 (100.0)	98 (100.0)	169 (100.0)
Base substitutions	69 (75.0)	87 (73.1)	77 (76.2)	25 (27.2)	20 (20.4)	62 (37.0)
A-T → G-C	6 (6.5)	7 (5.9)	5 (5.0)	5 (5.4)	5 (5.1)	7 (4.1)
G-C → A-T	18 (19.6)	31 (26.1)	28 (27.7)	7 (7.6)	11 (11.2)	30 (17.8)
G-C → T-A	29 (31.5)	32 (26.9)	22 (21.8)	11 (12.0)	3 (3.1)	18 (10.7)
A-T → C-G	3 (3.3)	3 (2.5)	5 (5.0)	1 (1.1)	0 (0.0)	4 (2.4)
A-T → T-A	7 (7.6)	4 (3.4)	6 (5.9)	0 (0.0)	0 (0.0)	1 (0.6)
C-G → G-C	6 (6.5)	10 (8.4)	11 (10.9)	1 (1.1)	1 (1.0)	2 (1.2)
Transitions	24 (26.1)	38 (31.9)	33 (32.7)	12 (13.0)	16 (16.3)	37 (21.9)
Transversions	45 (48.9)	49 (41.2)	44 (43.6)	13 (14.1)	4 (4.1)	25 (14.8)
One-base-pair frameshifts	15 (16.3)	11 (9.2)	15 (14.9)	58 (63.0)	78 (79.6)	106 (63.0)
ΔA/T	5 (5.4)	2 (1.7)	7 (6.9)	34 (37.0)	56 (57.1)	75 (44.4)
ΔG/C	3 (3.3)	6 (5.0)	5 (5.0)	3 (3.3)	18 (18.4)	15 (8.9)
+A/T	6 (6.5)	3 (2.5)	2 (2.0)	21 (22.8)	4 (4.1)	13 (7.7)
+G/C	1 (1.1)	0 (0.0)	1 (1.0)	0 (0.0)	0 (0.0)	3 (1.8)
Complex mutations†	8 (8.7)	21 (17.6)	9 (8.9)	9 (9.8)	0 (0.0)	1 (1.0)

Table S3. *CAN1* mutation spectra in *CDC9-OE* strains and *exo1*-mutants. Related to Figure 2.

Mutation spectra analysis based on DNA sequencing of the *CAN1* gene in independent Can^R mutants, shown as the number of clones containing the indicated mutations, and in parenthesis as the percentage relative to the total. **CAN1* mutation spectrum of WT strain was taken from [S7]. ** *CAN1* mutation spectrum of *msh2Δ* strain was taken from [S8].

† includes multiple mutations within ten nucleotides, insertions or deletions of more than one nucleotide and duplication events.

type	occurrence	length deletion/ insertion	*CAN1-ORF* (nucleotides)	length flanking sequence
deletions				
8/119 (7%)				
	1/119	16 bp	76-91	5 bp
	2/119	27 bp	284-310	8 bp
	1/119	49 bp	762-810	11/12 bp‡
	1/119	15 bp	1134-1148	6 bp
	1/119	63 bp	1286-1348	8 bp
	1/119	16 bp	1324-1339	4 bp
	1/119	39 bp	1625-1663	6 bp
insertions				
9/119 (8%)				
	1/119	32 bp	225-256	6 bp
	1/119	18 bp	290-307	4 bp
	1/119	33 bp	399-431	4 bp
	1/119	128 bp	688-815	none
	1/119*	49 bp	762-810	11/12 bp‡
	1/119	72 bp	1265-1336	7 bp
	1/119	50 bp	1384-1433	5 bp
	1/119	38 bp	1580-1617	6 bp
	1/119	32 bp	1667-1698	5 bp

Table S4. Complex deletions and insertions found in the *CDC9-OE* strain (*CAN1* mutation spectrum). Related to Figure 2.

* mutation reported in the *rad27Δ CAN1* mutation spectrum [S9]. ‡ the sequence of the upstream flanking repeat is GGTGCTGGGGT (11 nt) and the sequence of the downstream flanking repeat is GGTGCCTGGGGT (12 nt).

	Mutation Rate (fold increase)*		
Relevant genotype	**Lys$^+$**	**Thr$^+$**	**Can^R**
wild-type	1.5 [0.8-2.2] x 10^{-8} (1)	2.1 [1.4-3.2] x 10^{-9} (1)	7.2 [5.7-9.0] x 10^{-8} (1)
G2/M-MSH6 msh3Δ#	2.9 [1.7-4.7] x 10^{-5} (1983)	4.3 [3.3-5.5] x 10^{-6} (2069)	2.9 [2.1-4.3] x 10^{-6} (40)
G2/M-CDC9	8.0 [3.9-13.1] x 10^{-8} (5)	7.2 [4.8-10.0] x 10^{-9} (3)	4.0 [3.2-6.0] x 10^{-7} (6)
G2/M-MSH6 msh3Δ G2/M-CDC9	2.7 [1.7-3.9] x 10^{-5} (1813)	2.8 [1.5-4.1] x 10^{-6} (1330)	3.5 [2.2-4.8] x 10^{-6} (49)
G2/M-PMS1	6.1 [5.1-9.2] x 10^{-6} (418)	1.8 [1.3-2.4] x 10^{-7} (87)	5.9 [2.3-7.5] x 10^{-7} (8)
G2/M-PMS1 G2/M-CDC9	1.1 [0.8-1.5] x 10^{-6} (76)	4.2 [1.7-5.6] x 10^{-8} (20)	5.7 [4.3-10.1] x 10^{-7} (8)
G2/M-PMS1 cdc9-FFAA	2.8 [1.5-4.1] x 10^{-6} (194)	3.8 [2.7-6.5] x 10^{-8} (18)	2.1 [1.4-3.1] x 10^{-7} (3)
G2/M-PMS1 exo1Δ	4.6 [3.3-5.8] x 10^{-5} (3118)	2.1 [1.4-3.1] x 10^{-6} (991)	2.7 [1.9-3.2] x 10^{-6} (38)
G2/M-PMS1 lys2-10A$_{LATE}$	1.5 [1.4-1.9] x 10^{-6} (105)	1.2 [1.0-1.4] x 10^{-7} (59)	2.3 [1.8-3.4] x 10^{-7} (3)
G2/M-PMS1 exo1Δ G2/M-CDC9	2.3 [1.1-3.8] x 10^{-6} (157)	6.1 [4.4-8.0] x 10^{-8} (29)	1.4 [1.0-2.0] x 10^{-6} (20)
cdc9-FFAA	1.2 [1.0-1.7] x 10^{-8} (1)	3.4 [1.6-5.3] x 10^{-9} (2)	8.5 [7.3-17.3] x 10^{-8} (1)
G2/M-PMS1 exo1Δ cdc9-FFAA	7.8 [4.9-11.9] x 10^{-6} (536)	1.6 [0.9-2.4] x 10^{-7} (78)	1.1 [0.5-1.4] x 10^{-6} (15)
G2/M-PMS1 exo1Δ elg1Δ	1.2 [0.9-1.4] x 10^{-5} (794)	5.2 [3.4-9.4] x 10^{-7} (249)	1.8 [1.3-2.8] x 10^{-6} (26)

Table S5. MMR defect caused by the *G2/M-PMS1* allele is largely suppressed by delaying Cdc9 expression or reducing Cdc9 ligase activity. Related to Figure 4.
*Median rates of inactivation of the *CAN1* gene (Can^R) and *lys2-10A* (Lys$^+$) and *hom3-10* (Thr$^+$) frameshift reversion assays with 95% confidence interval in square brackets and fold increase relative to the wild-type in parentheses. # Mutation rates were taken from [S10].

Supplemental References

S1. Johnson, C., Gali, V.K., Takahashi, T.S., and Kubota, T. (2016). PCNA Retention on DNA into G2/M Phase Causes Genome Instability in Cells Lacking Elg1. Cell Rep *16*, 684-695.

S2. Kubota, T., Nishimura, K., Kanemaki, M.T., and Donaldson, A.D. (2013). The Elg1 replication factor C-like complex functions in PCNA unloading during DNA replication. Mol Cell *50*, 273-280.

S3. Kubota, T., Katou, Y., Nakato, R., Shirahige, K., and Donaldson, A.D. (2015). Replication-Coupled PCNA Unloading by the Elg1 Complex Occurs Genome-wide and Requires Okazaki Fragment Ligation. Cell Rep *12*, 774-787.

S4. Elledge, S.J., and Davis, R.W. (1990). Two genes differentially regulated in the cell cycle and by DNA-damaging agents encode alternative regulatory subunits of ribonucleotide reductase. Genes Dev *4*, 740-751.

S5. Kumar, D., Viberg, J., Nilsson, A.K., and Chabes, A. (2010). Highly mutagenic and severely imbalanced dNTP pools can escape detection by the S-phase checkpoint. Nucleic Acids Res *38*, 3975-3983.

S6. Williams, L.N., Marjavaara, L., Knowels, G.M., Schultz, E.M., Fox, E.J., Chabes, A., and Herr, A.J. (2015). dNTP pool levels modulate mutator phenotypes of error-prone DNA polymerase epsilon variants. Proc Natl Acad Sci U S A *112*, E2457-2466.

S7. Schmidt, T.T., Reyes, G., Gries, K., Ceylan, C.U., Sharma, S., Meurer, M., Knop, M., Chabes, A., and Hombauer, H. (2017). Alterations in cellular metabolism triggered by URA7 or GLN3 inactivation cause imbalanced dNTP pools and increased mutagenesis. Proc Natl Acad Sci U S A *114*, E4442-E4451.

S8. Buckland, R.J., Watt, D.L., Chittoor, B., Nilsson, A.K., Kunkel, T.A., and Chabes, A. (2014). Increased and imbalanced dNTP pools symmetrically promote both leading and lagging strand replication infidelity. PLoS genetics *10*, e1004846.

S9. Tishkoff, D.X., Filosi, N., Gaida, G.M., and Kolodner, R.D. (1997). A novel mutation avoidance mechanism dependent on S. cerevisiae RAD27 is distinct from DNA mismatch repair. Cell *88*, 253-263.

S10. Hombauer, H., Srivatsan, A., Putnam, C.D., and Kolodner, R.D. (2011). Mismatch repair, but not heteroduplex rejection, is temporally coupled to DNA replication. Science *334*, 1713-1716.